Print ISBN: 978-93-90206-53-7, eBook ISBN: 978-93-90206-54-4

Electrical Conduction in Doped Silicate Glasses (Thick Film Resistors)

Gulmurza Abdurakhmanov[1*]

DOI: 10.9734/bpi/nips/v4

ABSTRACT

Modern models of electrical conduction of doped silicate glass (thick film resistors) are reviewed and new approach to the problem is considered.

Keywords: Thick film resistor; doped silicate glass; electrical conduction; impurity band; electron-phonon interaction; nanocrystals; structure transitions; localization; hopping conduction.

1. INTRODUCTION

The silicate glass of various compositions, doped by oxides (oxide compounds) of transition metals (mainly Ru), is basic material for thick film resistors, resistor networks, electrical heaters and sensors of physical, chemical and biological factors [1-3]. This material is well known as thick film resistor, but we prefer to call it "doped silicate glass" (DSG) with this in the mind that thick film resistor is an electronic component ready for applications while DSG is a material only. Dopants are often called "conductive phase" for the reason that they have high electrical conductivity.

Despite the wide use of DSG, the mechanism of its electrical conduction was remained not well understood in many decades. For example variable range hopping, tunneling through potential barrier, thermal activation, effective medium approach and their combinations have been exploited [1], [4-10] to explain the temperature dependence of the DSG resistivity $\rho(T)$, schematically shown in Fig. 1. Unfortunately these models can describe $\rho(T)$ in the narrow range of low temperatures (regions I and II in Fig. 1) only. Such variety of approaches arises from inhomogeneity constitution of the DSG detected in X-ray diffraction patters and electronic microphotographs (Fig. 2) where one can see relict crystals of dopant distributed uniformly in the glass matrix.

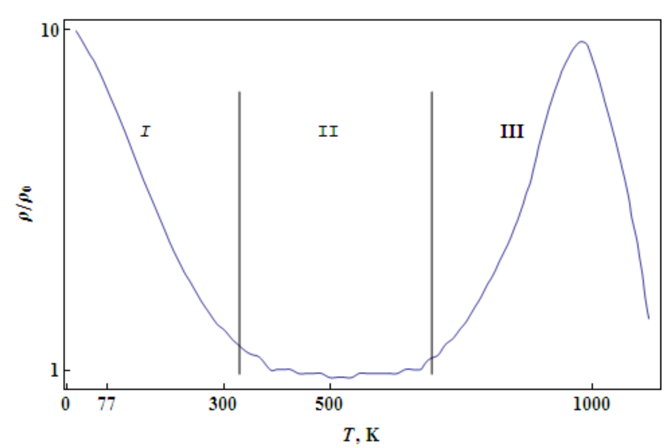

Fig. 1. Resistivity vs temperature for DSG (schematically)

[1]*National University of Uzbekistan, Uzbekistan.*
**Corresponding author: E-mail: gulmirzo@mail.ru;*

Regions I, II and III correspond to low, middle and high temperature.

Characteristic inhomogeneity scales in the DSG are followings [1-9]:

a) large scale inhomogeneity of few μm or larger, due to substrate, terminations and surface of sample;
b) middle scale inhomogeneity of 0.1 to few μm in size as result of mixing and sintering of powders of glass and dopant;
c) nanoscale inhomogeneity of 1 – 2 nm being characteristic for the glass itself.

Large scale inhomogeneities are dependent on the design of DSG sample mainly and too a much lesser extent on its volume.

Middle scale inhomogeneity consists in relict crystals of dopant (Fig. 2) and was the basis to consider the conduction of the DSG to be the percolation process caused by mutual contacts of relicts or hopping (tunneling) of charge carriers through the thin glass layer between them. Researchers mainly consider glass to be a passive matrix to fix the dopant particles (i.e. any interaction of dopant and glass is absent).

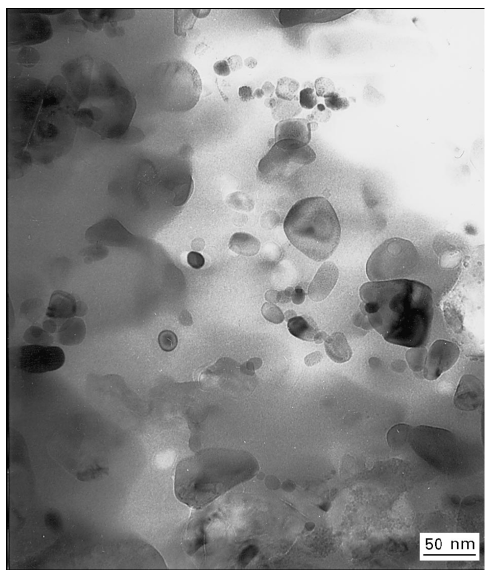

Fig. 2. Transmission electron microphotography of the DSG [17]

Nanoscale inhomogeneity was proposed by Lebedev in 1923, but has not considered in theories of DSG conductivity before 2011 [11], may be because of difficulties of their investigation. Moreover the existence of them in glass is the subject of the discussions up to date. So these two kinds of inhomogeneities do usually not considered as factors affecting the conduction mechanism of DSG.

There are quite a few questions which cannot be understood in the framework of the above-mentioned models:

a) how size and conductivity of the dopant particles affect the conductivity of DSG;
b) the mechanism by which it is affected by temperature T_f and the duration τ of the firing on the room temperature value of ρ_0 and slope of the $\rho(T)$;
c) why the glass composition affects the conduction of the DSG;
d) why the percolation threshold on the $\rho(C)$ shifts to small *C* or disappears for glass of various compositions;

e) what is the origin of the minimum of $\rho(T)$ and "metallic" state [12], observed beyond the $T_{\min}$, and etc.

Here $C = V_d/(V_d + V_g)$ is the volume fraction of the dopant in DSG or the doping level, V_d and V_g - volumes of the dopant and the glass accordingly, $V_0 = V_d + V_g$ is the total volume of the specimen.

A number of researchers [13-15] have claimed that the temperature dependence of resistivity of DSG near the minimum in the region II may be approximated by quadratic function.

$$\rho(T) = A(T - T_{\min})^2 + \rho_m \quad , \tag{1}$$

where ρ_m and $T_{\min}$ are the resistivity and the temperature at the minimum.

The dependence (1) as well as the maximum in the region III we have investigated [16] do not correspond to any known models of the electrical conductivity.

We examine these questions above from the position that the glass and the dopant interact in sintering process and electrical conduction of the DSG is the result of this interaction.

2. INTERACTION OF THE LEAD-SILICATE GLASS AND RUO$_2$

Some researchers have considered formation of "reactive layer" on the surface of the glass particles through the diffusion of dopant atoms [6] but effect of this layer on conductivity of DSG was not followed out. It was found by X-ray microanalyser in the model system of RuO_2 on the plate surface of the glass that Ru atoms diffuse into glass up to 1 µm in standard firing conditions ($T_f \approx 1123$ K, $\tau = 10$ min, total duration 60 minute). Unfortunately it was disregarded in this investigation that main diameter of the glass particles as well as thickness of glass layer between the relicts of the dopant is less than 1 µm, i.e. glass particles (layers) in DSG have doped through.

On the other hand silicate glass at standard firing conditions softens and becomes very aggressive substance, enable to solve appreciable amounts of oxides of many metals (units or tens of %) [17-19]. Moreover glass technology is based on the interaction of components at temperature high enough.

Interaction of RuO_2 and lead-silicate glass has been investigated [20] by X-ray diffraction, optical and infrared (IR) spectra methods.

2.1 Experiment

Samples investigated were powders of RuO_2, lead-silicate glass $2SiO_2{\cdot}PbO$, mixture of them before and after sintering in conditions standard for TFR technology. Powder particles were 0.2 µm and 0.5 µm in diameter for glass and RuO_2 correspondingly. Sintered mixture was milled up to 0.5 µm particle size too. Components used for glass melting were of technical category.

RuO_2 powders were made by thermal decomposition of $Ru(OH)Cl_3$ in air at 1100 K, milled and calcinated at the same temperature for 1 hour. There were no extraneous compounds of significant amounts found in the powder via XRD. Average size of particles in the powder was about 250 Å from Sherrer's formula, while the specific surface measurements give average size of about 0.5 µm. Therefore, one can assume the particles of powder investigated to be polycrystalline consisting from large number of crystalline regions oriented randomly. The discrepancy arises from gist of these methods. The Sherrer's formula gives main size of the region of coherent scattering (i. e. single crystalline region). On the contrary specific surface measurements give average open surface of the particles, from which main size of them will be calculated regardless of its internal structure (single crystal, polycrystalline etc.) so last value is always no smaller than first one.

IR absorption spectra of powders were taken on the IFS-113 Bruker Fourier spectrometer in the range of 2.5 – 100 μm, optical spectra – on the Specord M-40 (Karl Zeis, Jena) spectrometer in the 330 – 1050 nm range.

XRD patterns were taken on diffractometer DRON-UM-01 on CuKα radiation with graphite monochromator on reflected beam.

2.3 Results And Discussion

IR and optical absorption spectra of glass, RuO_2, mixture of them before and after sintering are shown in Fig. 3 [20].

Absorption bands near 10 μm and 22 μm on the IR spectrum of glass powder (Fig. 3*a*, curve 1) are due to vibrations of $[SiO_4]^{4-}$ tetrahedra and Pb-O bonds [21,22].

IR absorption spectrum of RuO_2 is featureless and absorbance is varied as λ^{-1} (Fig. 3*a*, curve 2). This means that atomic absorption is suppressed by that of free charge carriers, and $\omega << \omega_p$, where

$$\omega_p = \sqrt{\frac{ne^2}{m^* \varepsilon_0}} \tag{2}$$

is plasma angular frequency, n and m^* are concentration and effective mass of free carriers, ε_0 is the permittivity of vacuum [23].

IR spectrum of mixture of glass and RuO_2 powders before sintering is superposition of appropriate spectra (Fig. 3*a*, curve 3) and do not have new absorption bands. The character of the spectra changes after sintering (Fig. 3*a*, curve 4): absorption increases at $\lambda > 10$ μm and the wavelength dependence is stronger, new absorption bands appear at 6.6 μm and 12.5 μm. The latter one overlaps with the long-wavelength wing of intensive band at 10 μm. Absorption by free carriers is still dominant in the region of $\lambda < 9$ μm and $\alpha \sim \lambda^{-1}$.). Here μ is absorbance (arbitrary units), λ and $\tilde{\nu}$ are wavelength and wave number accordingly in these spectra.

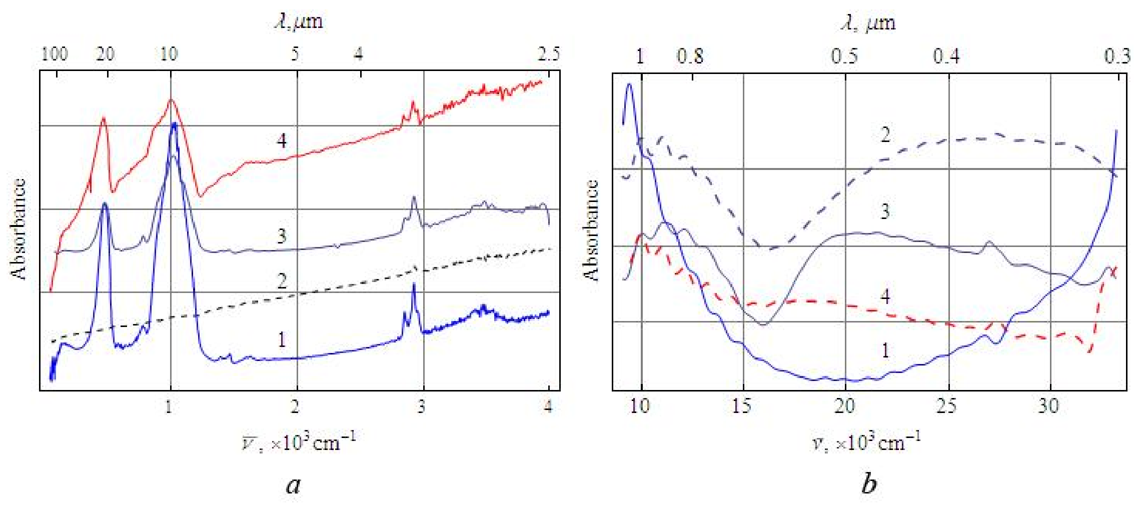

Fig. 3. IR (*a*) and optical (*b*) spectra of powders: glass (1), RuO_2 (2), mixture of them before (3) and after (4) sintering

Optical spectrum of glass powder (Fig. 3*b*, curve 1) is typical and shows the fundamental absorption band starting at 350 nm (transitions from valence band to conductive band) inherent to glass containing 33 mol. % of PbO [24].

Optical spectrum of RuO_2 powder (Fig. 3*b*, curve 2) has two wide absorption bands centered at 360 and 950 nm (location of last one is approximated because of existence of fine structure).

Optical spectrum of the mixture of powders before sintering (Fig. 3*b*, curve 3), like the IR spectrum, is the superposition of spectra of initial powders and does not have additional peculiarities.

The absorption band at 950 nm of optical spectrum of sintered mixture (Fig. 3*b*, curve 4) is slightly shifted to highest wavelength and band at 360 nm almost disappears.

It should be noted that in contrast to single crystals, the powders of RuO_2 used by us are semiconducting (Fig. 4). This might be due to the excess oxygen atoms on the surface of particles. These measurements were made on pellets pressed at 800 MPa, when resistivity becomes nonsensitive on applied pressure.

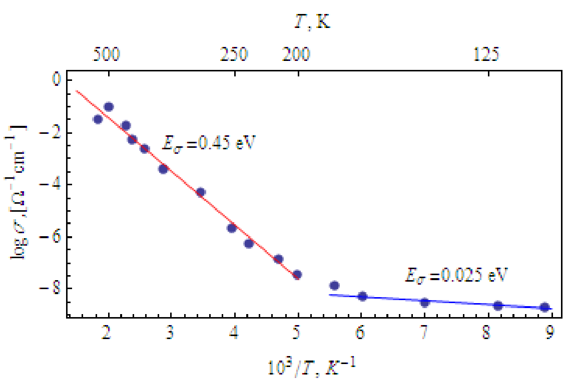

Fig. 4. Temperature dependence of electrical conductivity of RuO_2 pellet

Activation energy determined as a slope of $\sigma(T)$, has two values: 0.45 and 0.025 eV. Higher value could be attributed to the oxygen layer on the surface of particles which makes them semiconductive, and smaller value is the property of the particle volume.

So one can relate the band 360 nm to the surface layer (transitions between Ru 5s and O 3s states with transition energy of ~3 eV) and band 950 nm – to plasma resonance of free carriers. Thus, it follows from (1) that n has decreased from $1.2 \cdot 10^{21}$ cm^{-3} to $1.1 \cdot 10^{21}$ cm^{-3} due to sintering.

Gas of free carriers of same concentration is degenerated and temperature dependence of the resistivity of DSG obeys the power-law ($\rho \sim T^k$) in accordance with scattering mechanism.

Density of RuO_2 molecules is $3.6 \cdot 10^{22}$ $см^{-3}$ and there is only one electron per 30 atoms of Ru (see above) in RuO_2 powder at room temperature. On the other hand one can assume that all Ru atoms diffused into glass are ionized and concentration of free carriers in TFR is equal to that of Ru atoms. Intensity of the main lines of X-ray diffraction of RuO_2 in mixture of glass and RuO_2 powders after firing decreases up to 90% of that in the nonfired mixture. Since volume content of RuO_2 in mixture was 16% (corresponds to 25 weight %) one can consider that only small part of Ru atoms (nearly 3%) is diffused from particles into glass.

Paucity of Ru atoms diffused into glass is verified from X-ray diffraction patterns as well (Fig. 5). Main reflexes of RuO_2 in last one are broadened and shifted slightly to small angle after sintering. This means that the relicts of RuO_2 crystals are stressed in TFR because of the highest value of thermal expansion coefficient of RuO_2 crystals in the *a* direction in comparison to that of glass ($144 \cdot 10^{-7}$ K^{-1} and $71 \cdot 10^{-7}$ K^{-1} accordingly), while in the *c* direction it is negative ($-39 \cdot 10^{-7}$ K^{-1}).

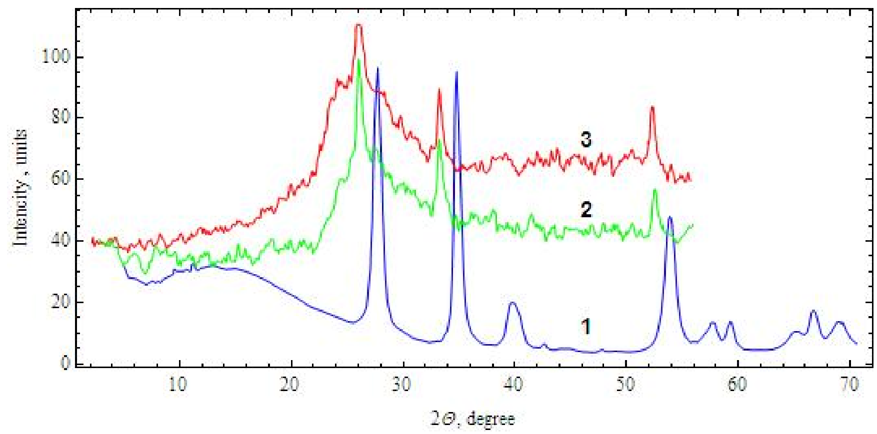

Fig. 5. X-ray diffraction in RuO_2 (1) and DSG (glass + 16 mass. % RuO_2), sintered at 873 K (2) and at 1073 K (3)

New bonds O-Ru-O form during the sintering process in addition to the existing Si-O-Si (bridge atoms of oxygen) and O-Pb-O bonds, inherent in glass $2SiO_2{\cdot}PbO$. Additional bonds have large dispersion of length and bonding constant because the diffused atoms of Ru became bonded both to the $[SiO_4]^{4-}$ tetrahedra and Pb atoms, generating the Si-O-Ru-O–Si, Si-O-Ru-O-Pb-O and O-Pb-O-Ru-O-Pb bonds. Retained bonds O-Ru-O-Ru-O are deformed due to the mismatch of thermal expansion of RuO_2 and glass. Since the atomic mass of Ru lays between that of Si and Pb, the bonds of Ru with oxygen atoms, having different location in glass structure, appear as wide absorption band between 10 and 22 µm (Fig. 3*a*).

3. DIFFUSION AND PERCOLATION IN DSG

So long as firing duration of DSG is limited (usually $\tau \approx 10$ min) and mechanical mixing is not applied, the distribution of solved atoms of the dopant in the glass should be diffusive only.

The production of specimens is a standard procedure for thick film resistors and is described in many papers and books (see, for example, [1]). The glass compositions used are as follows (weight %):

Glass1 SiO_2 31; PbO 67; MnO_2 2;
Glass2 SiO_2 29; PbO 67; BaO 4.

The DSG specimens compositions are as follows (weight %):

1. Glass1 80; $Pb_2Ru_2O_6$ 20;
2. Glass1 90; RuO_2 10;
3. Glass2 90; RuO_2 10;
4. Glass2 80; RuO_2 20.

Volume fraction of dopant C is less than theoretical percolation threshold (critical value C_c) in all cases.

3.1 Diffusion and Formation of Percolation Levels - Experiment

The percolation theory is considered as most common model of conduction mechanism of the DSG [25-27]. This theory assumes that transport of charge is realized through the conductive chains formed by mutual contacts of relicts of dopant particles, having high conductivity, or through chains of these particles, separated by thin glass layers, via tunneling (hopping) of carriers. But one needs to know *a priori* volume fraction of conductive particles C to apply the theory, and this value is often defined as $C = \gamma_g m_d/(\gamma_g m_d + \gamma_d m_g)$, where m_d and γ_d are mass and specific weight of the dopant in initial (before firing) composition of DSG, m_g and γ_g are same values for the glass. According mass fraction of a dopant is $C_m = \gamma_d C/(\gamma_d C + (1 - C)\gamma_g)$. It means that one neglect any interaction of dopant and glass in calcination.

The main statement of the percolation theory is formation of a single infinite conductive cluster for $C \approx C_c$, which fills uniformly whole volume of a sample. C_c is the critical volume fraction of the dopant below which resistivity of system ρ goes to infinity:

$$\rho(C) = \rho_0 (C - C_c)^{-t}, \tag{3}$$

here ρ_0 is material-dependent prefactor, t is the dc transport critical exponent. According to the standard theory of transport percolation [24], $C_c \approx 0.12 - 0.39$ and $t = t_0 = 1.6\text{-}2$ is the universal value in the problem of bonds for three-dimensional disordered composites.

We have tested the statement above experimentally by laser cutting out the DSG sample with $C \approx 16\%$ ($C_m \approx 27.5$ mass % for RuO_2) along the current streamlets (lines 4 in Fig. 6*a*), and have not found any abrupt change in resistance (Fig. 6*b*), characteristic for breaking of single cluster. In contrary the resistance increased as the number of grooves *n*, testifying geometrical effect only.

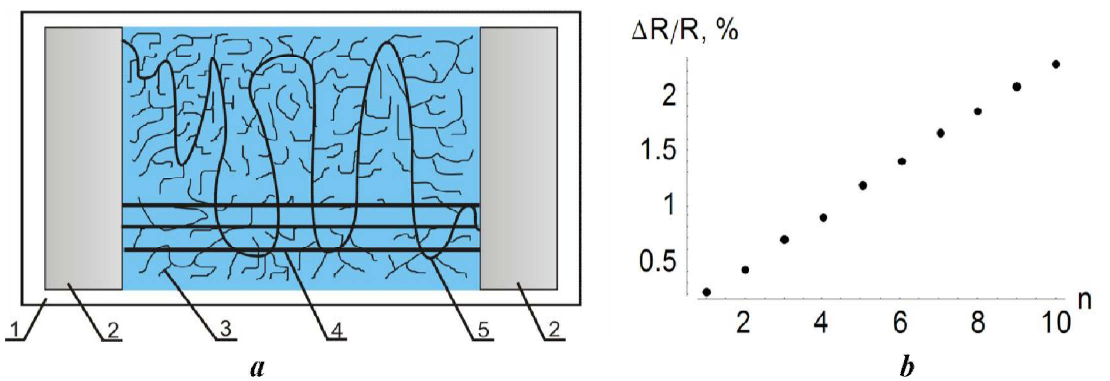

Fig. 6. Laser cut of the DSG (*a*) and change of resistance Δ*R* of DSG vs. number *n* of grooves (*b*). 1 – ceramic substrate, 2 – metallic terminals, 3 – DSG layer and dead ends, 4 – grooves, 5 – single infinite cluster

The expression (3) predicts a percolation threshold of $\rho(C)$ at $C \approx C_c$, while in reality the value of t might be as high as 7 for various compositions of glass and doping conditions [28]. Additionally, the value of C_c is essentially lower than the theoretical estimation in many cases or percolation threshold disappears.

The reason for this discrepancy between the experimental results and the theory of percolation is the assumption that the volume fraction C of the dopant in the DSG (after firing) is known *a priori* (often it equals to the initial volume fraction of them). In fact the interaction of dopant and the glass is possible during the firing process as well as the mutual diffusion of the glass and dopant atoms. As the result one does not have information about C in the final stage of technological process and about the value of the resistivity of doped regions of the glass.

So we should consider that the glass resistivity (in the diffusion zone) is reduced by many orders of magnitude due to diffusion (as in crystalline semiconductors) and infinite cluster consists of closed or overlapping diffusion zones which have been formed around the each dopant particle (Fig. 7).

Let us to consider [29] that the diffusion zone is spherical because the glass is isotropic. This diffusion zone has the volume

$$V_\mathrm{d} = \frac{4\pi}{3} R_\mathrm{d}^{\;3}, \tag{4}$$

There $R_\mathrm{d} = r + l_\mathrm{d}$ is the radius of the diffusion zone, *r* is the main radius of the dopant particles, and the diffusion length is

$$l_\mathrm{d} = \sqrt{D\tau} = \sqrt{D_0 \tau}\exp(-\frac{E_\mathrm{d}}{2kT_\mathrm{f}}). \tag{5}$$

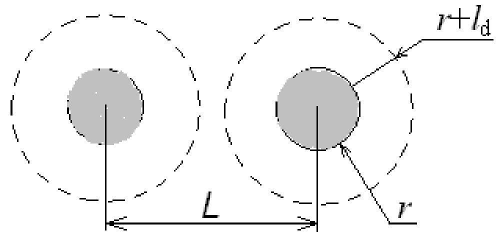

Fig. 7. Formation of diffusion zone around the dopant particle of the radius *r*. There *r*+*l*$_\mathrm{d}$ is the radius of diffusion zone, *l*$_\mathrm{d}$ is the diffusion length. *L* is the main distance between the neighbor dopant particles in the DSG

There *D* is the diffusion coefficient, $D_0 = D(T_\mathrm{f} \to \infty)$, E_d is the activation energy of diffusion, and *k* is the Boltzmann constant. Inserting $C = V_\mathrm{d} / (V_\mathrm{d} + V_\mathrm{g})$ and $C_\mathrm{c} = V_\mathrm{c} / (V_\mathrm{d} + V_\mathrm{g})$ into (3) and taking into account (4) and (5) gives

$$\ln\{[\frac{3V_0}{4\pi}((\rho / \rho_0)^{-1/t} + V_\mathrm{c} / V_0)]^{1/3} - r\} = -\frac{E_\mathrm{d}}{2kT_\mathrm{f}} + \frac{1}{2}\ln(D_0\tau).. \tag{6}$$

Expression (6) for $\rho(T_\mathrm{f})$ of DSG is in a good agreement with experiment (Fig. 8) for various glasses and dopants and makes it possible to evaluate D_0, E_d and l_d from the experimental data (Table 1, [29]). Here ρ_0 is the fitting parameter and corresponds to average resistivity of the diffusion zone, which is unknown and is Usually no uniform. The value of the diffusion length $l_\mathrm{d} \approx$ 0.22 – 1600 µm, evaluated in the same manner for the standard firing conditions is essentially higher than the main distance between dopant particles

$$L = 2r\sqrt[3]{\frac{\pi}{6C}} = 2r\sqrt[3]{\frac{\pi}{6}[1 + \frac{\gamma_\mathrm{d}}{\gamma_\mathrm{g}}(\frac{1}{C_\mathrm{m}} - 1)]}. \tag{7}$$

From (7) we have $L \simeq 0.16$ µm for main diameter $2r \approx 0.1$ µm of dopant particles and volume fraction $C \approx 0.16$, so diffusion zones are heavily overlapped and the whole volume of the specimen is uniformly filled by infinite conductive cluster, as shown schematically in Fig. 9.

Table 1. Diffusion coefficient D_0, activation energy E_d and diffusion length l_d, evaluated from Fig. 8

Specimen of DSG	E_d, eV	D_0, cm^2/s	l_∂, cm, at T_f = 850˚C
1	1.08	$5.65 \cdot 10^{-8}$	$2.2 \cdot 10^{-5}$
2	0.624	$9.48 \cdot 10^{-6}$	$3.0 \cdot 10^{-3}$
3	0.194	$5.74 \cdot 10^{-4}$	0.125
4	0.212	$4.1 \cdot 10^{-4}$	0.166

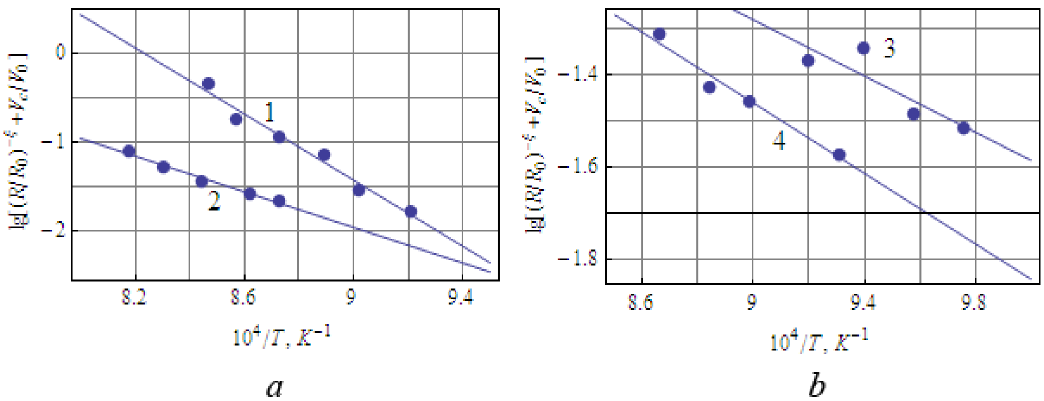

Fig. 8. $R(T_f)$ for DSG mentioned above (see Introduction). Solid lines are fitting of (5) to experimental data by the least squires method

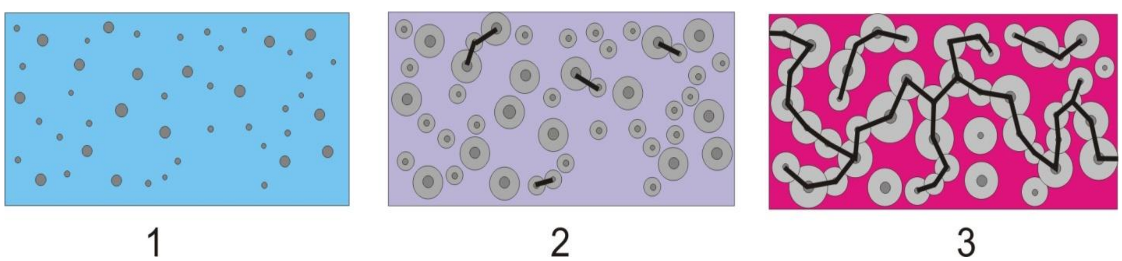

Fig. 9. Generation of percolation levels due to diffusion (schematically). The bold curve is the infinite cluster. Gray circles represent diffusion zones. T_f in 3 is higher than in 1. τ = const

Expression (6) shows good agreement with the experimental data for DSG of other compositions [30] as well (Fig. 10*a*).

One can also derive the effect of firing duration τ on the resistivity ρ of DSG from (3) – (5):

$$\tau = \frac{1}{D(T_f)} \left[\sqrt[3]{\frac{3}{4\pi}[V_0(\rho_0/\rho)^{1/t} + V_c]} - r \right]^2 . \qquad (8)$$

This expression is compared with the experiment in Fig. 10*b*.

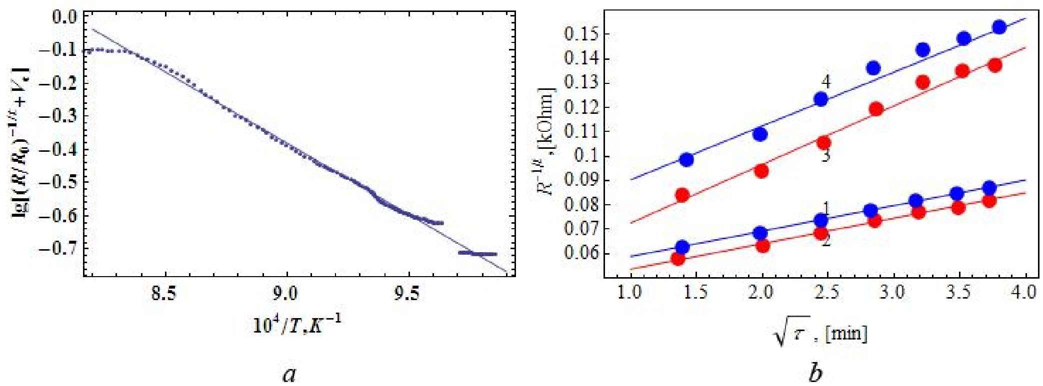

Fig. 10. (*a*) $R(T_f)$, recalculated data from [30] in accordance with (6). The solid line is fitting of (6) with R_0=10 Ohm, t=1.7, V_c=0.16; (*b*) $R(\tau)$ for DSG at T_f, K: 1073 (1, 2) and 1123 (3, 4). Temperature increasing rate is higher for data 1 and 2, than for data 3 and 4. Points are recalculated from [30] in accordance with (7). DSG composition isn't varied

We have simulated the effect of doping level and size of dopant particles on the ρ of DSG. The simulation is based on Fick's equation [31] and expression (7). It is assumed that 1) diffusion from neighbor particles of the dopant into the glass interlayer is uniform; 2) value of ρ is predetermined by minimum of concentration N of dopant atoms at the middle point being at distance L/2 from each of them, i. e.

$$\rho \propto N^{-1}(x = L/2). \quad (9)$$

The result of the simulation of $\rho(\tau)$ for two sizes of dopant particles is shown in Fig. 11*a*. There is exponential dependence characteristic for usual diffusion. It is clear on one hand that the size of dopant particles essentially affects on the conductivity of DSG. On the other hand $R(\tau)$ at small τ is stronger in our simulation than in the usual model of diffusion $R(\tau) \propto \exp(-c\sqrt{\tau})$ (the dotted line in Fig. 11*a*) (the last is shown in Fig. 10*a* as dotted line fitted to model curve *a* in the three points).

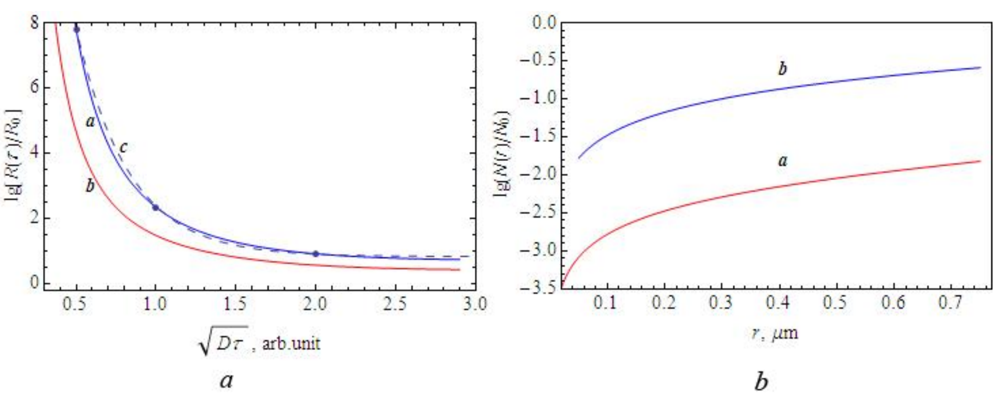

Fig. 11. (*a*) Simulation of $R(\tau)$ of DSG for *r*, μm: 0.5 (*a*); 1 (*b*); the function $a + b\exp(-c\sqrt{\tau})$ (dotted line). $L \approx 5$ μm. (*b*) Effect of the main size *r* of dopant particles on resistivity of model DSG ρ ~ N^{-1}(x/2) (simulation, see Fig. 6 and 11). *C* for curve *a* is 2 times less than for curve *b*.

The *τ* accords to l_d = $\sqrt{D\tau} = 1{,}25$ μm.

Resistivity of DSG is strongly affected by the dispersivity of the dopant powder [29] – reduction of the diameter of the particles from 4.5 μm down to 1.6 μm decreases the resistivity by bout one order in magnitude. We have simulated this effect as the result of diffusion process (Fig. 11*b*) in accordance with the expression (5) for two values of $C < C_c$. There we have used the assumption (9) as well. One can see that the dependence $\rho(r)$ or $N(r, x = L/2)$ becomes stronger for smaller r, when the main distance between dopant particles have been decreased for constant C, and conductivity of the DSG increases.

It must be noted here that the information on the solubility of RuO_2 in lead-silicate glass is contradictory: Palanisamy et al. [32] estimate it less than 10^{-4} atomic %, while Flachbart et al. [8] present the value about 7 atomic %. We are inclined to admit the last value because of the results of X-ray diffraction experiments, in which the intensity of main reflexes of RuO_2 relicts in DSG reduces nearly 10 % due to firing and they become wider [20]. One should also take into account the fact that solubility of pure metals in silicate glass is very small (really less than 10^{-3} atomic %, [33]), while solubility of their oxides is essentially higher (up to 10 – 70 mol. % for PbO).

It is clear in the same approach that the electrical properties of DSG, specifically $\rho(r)$, beyond the formation of infinite cluster of diffusion zones, mainly depend on the properties of the doped glass, namely, on the glass structure, on the distribution of the energy levels of the impurity in the energy gap of the glass, and on other microscopic characteristics.

The resistivity of the glass in the diffusion zone may be estimatedas 5 - 6 orders of magnitudes higher than that of the dopant relicts, so the latter one does not affect the macroscopic parameters of the DSG unless they form an infinite cluster (i. e. unless $C < C_c$). Indeed, the conduction is metallic at $C > C_c$, where electrical conduction of DSG supported by mutual contacts of dopant particles.

Unfortunately this model is not enough to explain origin of minimum of $\rho(r)$ at middle temperatures (region II in Fig. 1) and its maximum at high T (region III in Fig. 1).

4. NANOCRYSTALS AND IMPURITY BAND [11]

A detailed study of the influence of various experimental parameters (temperature, RuO_2 content, stirring, etc.) on the electrical conductivity and, in particular, on the percolation threshold in borosilicate glass–RuO_2 composites is presented in [34]. This percolation threshold is shown to increase by a factor of two (from 0.6 to 1.2 vol %) when stirring is applied during synthesis and by more than a factor of three (> 2.1 vol%) when a sol–gel route is used. Besides, the study of various synthesis temperatures reveals that the electronic part of the electrical conductivity is highly correlated to Ru solubility in the glass matrix. It was concluded from these experiments that both the presence of dissolved ruthenium in the glass matrix and the possibility of RuO_2 particles to rearrange in the melt in order to form kind of a network are necessary for a low percolation threshold. The last conclusion is erroneous because of the considerable deviations of resistivity values of samples estimated for such network of RuO_2 particles and measured experimentally for same volume content of RuO_2.

Jagtap et al. [35] have added some compounds into the thick film composite (glass+conductive phase) to reduce the temperature coefficient of resistivity, but the mechanism of this effect did not explained.

Low frequency noise spectroscopy is employed in [36] to examine fluctuating phenomena that take place in the material of resistive films and in the film/termination interface of a thick-film resistor. It has been found that the excess low frequency noise apart from the 1/f component contains contributions from thermally activated noise sources with energies in the range 0.015–0.6 eV. These sources are considered to be distributed nonuniformly over the whole resistor volume, most probably in the glassy matrix or conductive grain boundaries.

It was confirmed [37,38] that the diffusion of ruthenium into glass affects the binding state of RuO_2 at the interface of the glass. Furthermore, an intermediate resistive layer is detected around the RuO_2 particle. These results suggest that the piezoresistive effect is related to change in the electrical conductivity of the interfacial reaction layer caused by the diffusion of Ru into glass. Authors assert that their results may be explained by variable hopping model.

Hill [39] has proposed forming of a narrow band in forbidden gap in the glass without any consequence applicable to explain observed properties.

Unfortunately, in all these works as well as in earlier investigations [6,7] suggested interactions of the glass and the conductive phase (mainly RuO_2) were not summarized into the detailed model of conductivity of the DSG and the effect of nanoscale glass structure was not considered.

4.1 Nanocrystals in the Glass and Localization of Charge Carriers

Metastability of glassy state is widely accepted [40] and all kinds of glasses will become crystalline with time. The time required for this transition may be many years or even millennium depending on its composition and thermal prehistory, i. e. depending on the height of potential barrier, separating these two states.

Crystals are formed spontaneously in the glass so the Helmholtz energy of the crystalline state is lower than that of the glassy state of same composition. It means that these crystals act as pockets of potential energy (Fig. 12). The silicate glass is dielectric with energy gap as high as 3.3-7 eV (the glass $2SiO_2 \cdot PbO$ and fused silica accordingly). On the other hand natural crystallization of the silicate glass is very slow (usually tens of years), and relevant energy of this process is insignificant. Because of this one can assume that the pockets are not deep (of about 0.01 – 0.03 eV) and dynamical balance of transitions from glassy state into crystalline state and back is slightly disturbed in the line of first.

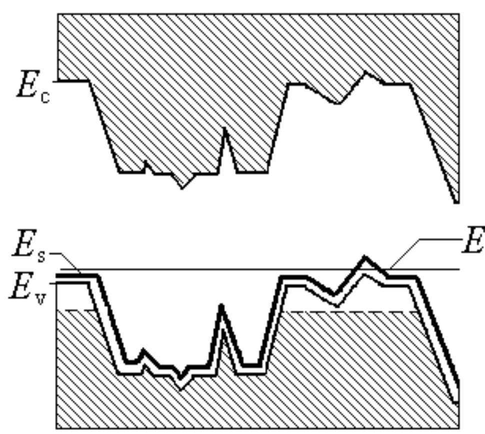

Fig. 12. Energy pockets of nanocrystals in the glass, impurity band and the regions of free carriers localization. E_c and E_v are the conductivity and the valence bands of the glass accordingly, E_s is the impurity band, E_p is the percolation level

Free charge carriers in DSG are holes as it is indicated by the sign of the thermopower [4]. Concentration of them is about 10^{20} cm^{-3} and the effective mass m^* is about 330 m_0 (m_0 is mass of the free electron) as it was estimated from the resistivity ρ and the upper limit of mobility μ of DSG [41]. The increase of effective mass of electrons (holes) in the small size pockets have been demonstrated in [42] for GaN.

The bottom of the conduction band of the lead-silicate glass is formed by the shifted 3*s*-orbitals of the oxygen and 6*d*-orbitals of the lead, while the top of the valence band is formed by shifted 2*p*-orbitals of O_2 and 6*p*-orbitals of Pb [43]. As a result, lead-silicate glass is the dielectric with the band gap about 3.3 eV [44], and the silica glass has $E_g \approx 7.76$ eV [45], since the conduction and valence bands are formed by shifted 3*s*- and 2*p*-orbitals of O accordingly. Doping of the lead-silicate glass forms the impurity band from shifted 5*s*-states of Ru atoms. 6*p*-states of Pb and 5*s*-states of Ru are shifted to 7.415 eV and 7.36 eV below the vacuum level (first ionization potential, [46]) accordingly. Displacement of the impurity band in the forbidden gap of the glass is shown schematically in Fig. 13*a*. It is known that conductivity of DSG varies very slowly in the wide temperature range and the photoconductivity do not appears up to the ultraviolet, where transition of electrons from the valence band into the conduction band takes place. So one can say that ruthenium band abutted to top of the valence band of glass or slightly (less than 0.01 eV) separated from the last one (Fig. 13*b*) at room temperature. Then the Fermi level E_F appears as close to the top of the valence band as 0.01 eV or less and the gas of free carriers is degenerated at room temperature.

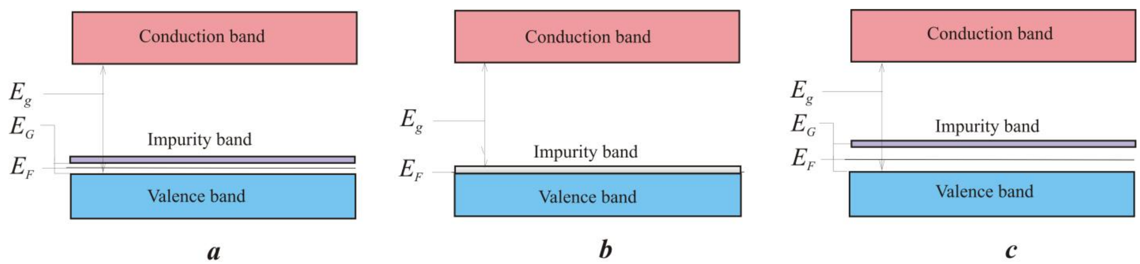

Fig. 13. Energy bands and the band-gap E_G in DSG at temperatures *T* (schematically, K): 0 (*a*), about 300 (*b*) and > 900 (*c*)

This is confirmed by IR and optical spectra of DSG (Fig. 3**)**. We assume that the arms at 50 μm ($h\nu \approx$ 0.026 eV) and at 12 μm ($h\nu \approx$ 0.1 eV) on the IR-spectrum of DSG (Fig. 3*a*, curve 4) correspond to the electron transitions from the glass valence band into the impurity band because they are not characteristic neither of glass (Fig. 3*a*, curve 1) nor of RuO_2 (Fig. 3*a*, curve 2), and shoulder at 12 μm can be caused by transitions from the pockets generated by nanocrystals into the impurity band (Fig. 12). So one can estimate the depth of the pockets as 0.1–0.025 = 0.075 eV.

At high temperatures (region III in Fig. 1) nanocrystals of silicates in the DSG undergo structural transitions, leading to increasing of interatomic distance about 2%, so overlapping of electronic wave functions exponentially decreases. As a result impurity band shifts far from valence band of glass and one has typical semiconductor (Fig. 13*c*). Forbidden gap of this semiconductor depends on DSG composition and varies in interval 0.09-1.5 eV (see below, Figs. 16 and 20).

4.2 Temperature Dependence of Conductivity of the DSG

Coexistence of glassy and crystalline sections (and potential energy pockets as accordingly) in DSG as well as narrowness of the impurity band and its proximity to the top of the glass valence band leads to the following [11]:

1) All the states in the impurity band are ionized at room temperature, gas of carriers is degenerated and the temperature dependence of the conductivity of DSG $\sigma(T)$ is very weak;
2) Particularly, at low temperatures when the impurity states are less ionized, the simultaneous action of the activation and hopping mechanisms of conductivity in DSG is possible, so the total conductivity is

$$\sigma(T) = AT\exp(-E_g(T)/2kT) + BT^{0.5}\exp(-(T_0/T)^{1/4}), \qquad (10)$$

where the first term corresponds to the activation mechanism with the activation energy $E_g(T)$ and the second term corresponds to the variable range hopping (Mott's low [47]). *A* and *B* are constants depending on the relative volumes of glassy and nanocrystalline sections, *k* is the Boltzmann's constant, T_0 is the some constant ($T_0 \sim 10^6$ K).

There are two problems. The first one caused by the possibility of experimental corroboration of the Mott's low (5). It has been showed [48] that the second term in (10) in the generalized form

$$\sigma(T) = AT^n \exp\left[-(T_{\mathrm{h}}/T)^m\right]$$

can be in good agreement with the experimental data in the wide range of m = 0.2 – 0.55 for appropriate choosing of n in the interval -7.5 to 2.75. Despite it this expression with various values of n is used often as the proof of the hopping conductivity in the DSG.

The second problem is the result of the fact that carriers hopping (which is actually the quantum-mechanical tunneling) is not effective in distance about 0.1 – 1.5 μm that corresponds to mean distance (7) between the dopant particles in the DSG. It forces the researchers to consider the diffusion of dopant atoms into the glass or the particles to be far smaller than they are actually.

Authors [8] as well as Schoepe [7] have derived experimentally for DSG conductivity at low temperatures (0.05 – 2 K) the expression

$$\sigma(T) \sim \exp[-(\Theta/T)^x] \tag{11}$$

with x = 0.5 and explained it as result of tunneling though graded barriers. For x = 0.5 one finds p = 2 in three dimensions (d = 3), and this value corresponds to the density of states variations expected to result from Coulomb interaction between localized carriers [27]. Here d is the dimensionality and p is the power by which the density of states $N(E)$ rises about the Fermi level: $N(E) = |E - E_{\mathrm{F}}|^p$. Subsequently these authors [8] have calculated for mentioned experimental results the localization radius $a_0 = e^2/(\varepsilon\varepsilon_0 kT_{\mathrm{h}})$, here e is the electron charge, ε_0 is the permittivity of free space, ε = 10 is the static dielectric constant of DSG. It was found that $a_0 \approx 2$ μm and the estimated activation energy less than kT. Such value of a_0 is meaningless because of the mean size of the dopant particles where carriers to be localized is about 0.1 – 1 μm. So authors [34] conclude that the percolation theory is not applicable to the DSG.

It was concluded in [49] that hopping mechanism is important at low temperatures and tunneling takes place at high T.

The activation energy in (10) depends on temperature [50] as

$$E_g(T) = E_{g0} - \xi\langle\hbar\omega\rangle(\mathrm{cth}\langle\hbar\omega\rangle/kT) - 1), \tag{12}$$

here E_{g0} is the activation energy at T = 0 K, ξ is the dimensionless constant of electron-phonon coupling and $\langle\hbar\omega\rangle$ is an average phonon energy. So the equation (10) can be fairly well approximated by

$$\sigma(T) = \sigma_0 T^{0.5} \exp(-(K/T)^{\varsigma}) \tag{13}$$

with 0.4 < ς < 0.8 as often observed in experiments. Fig. 14 shows that it is problematic to discriminate equations (10) and (13) experimentally.

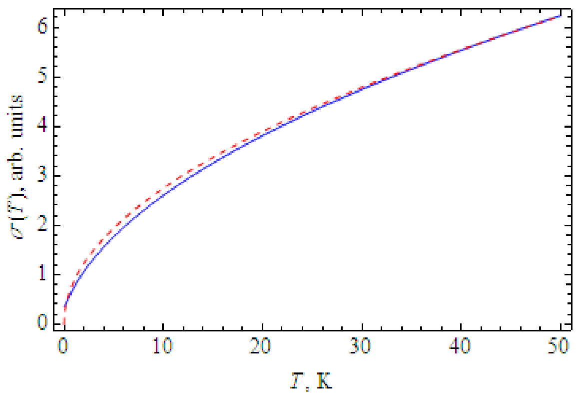

Fig. 14. Comparison of expressions (10) (dotted line) and (12) (solid line) at: A = 10^{40}; B = 3.5; T_0 = 100 K; $E_{\sigma0}$ = 10^{-2} eV; ξ = 1.1; $\langle\hbar\omega\rangle$ = 22.5 K; σ_0 = 1.67; K = 10 K; ς = 0,5

The value of activation energy E_g = 10^{-2} eV derived from the fitting process of the eq. (10) to the eq. (13) also confirms that impurity band is displaced close to the top of the glass valence band.

3)Silica SiO_2 has some crystalline modifications which can undergo the structural transitions [40,51]. In addition structural transitions are possible in the nanocrystals of silicates at high temperatures when interatomic distances vary suddenly and it must result in the reduction of the conductivity of DSG analogous to ferroelectrics [52].

The sharp decrease of the conductivity of DSG we have observed (Fig. 15) at sufficiently high temperatures [11] and the starting point of this process depend on the glass composition. But further increase of temperature leads to the increasing of σ with the activation energies about 0.095–1.52 eV depending on the glass composition (Fig. 16). This means that the impurity band splits off the glass valence band at T > 800 K because of structural transitions of nanocrystals and narrow energy gap forms between them (Fig. 12*c*). The thermal generation of free carriers takes place through this gap and DSG turns into a typical semiconductor. It should be noted that the structural transitions in nanocrystals consisting of silicates do not occur suddenly but occupy some temperature interval. At the beginning of this interval nuclei of the new phases are generated and they accumulate gradually until whole sample transits into a new phase at the transition point (at the end of the temperature interval) [53].

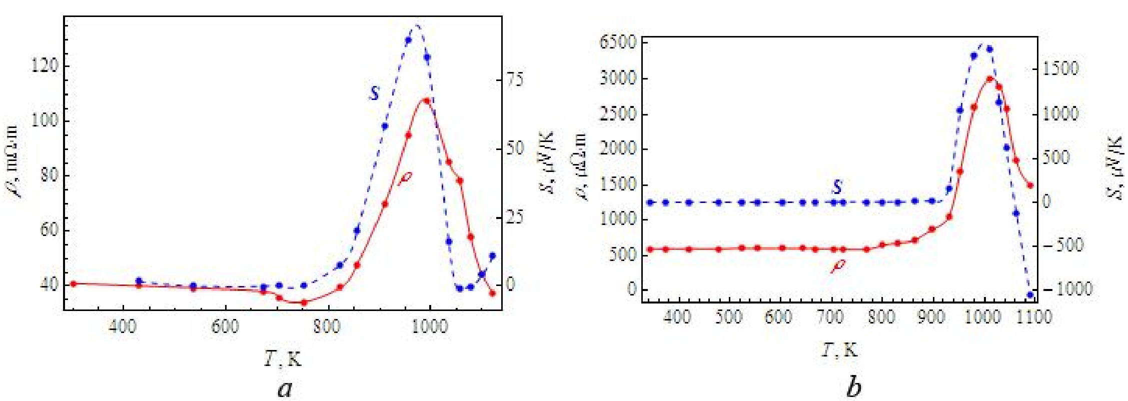

Fig. 15. Temperature dependence of the resistance ρ and the thermopower S of DSG based on the glass1 (*a*) and glass2 (*b*)

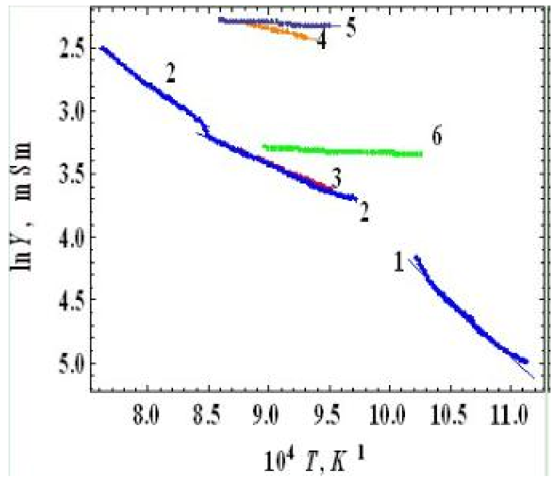

Fig. 16. Temperature dependence of the conductivity *Y*(*T*) after minimum for the samples of the doped glass1 (1) and glass2 (2 – 6) with RuO_2 content about 16 wt % (1, 2), 20 wt% (3, 4) and 30 wt % (5, 6). Activation energy of conductivity E_σ is about (eV): 1.77 (1); 1.54 (2, lower *T*) and 0.93 (2, high *T*); 0.9 (3); 0.52 (4); 0.05 (5) and 0.047 (6). The solid lines are the fit of the experimental data to the expression $\ln Y = a + E_\sigma / 2kT$

The value of the thermopower S of the DSG corresponds to that of metals (about 10 μV/K) and its temperature dependence confirms that the concentration of charge carriers does not change significantly in the 300 K < T < 800 K interval (Fig. 16). At the temperature corresponding to the minimum of $\sigma(T)$ the modulus of S increases sharply and reaches up to 1 mV/K for the DSG of various compositions.

This indicates as well the decrease of the concentration of carriers. Beyond the minimum of $\sigma(T)$ value of S reduces in accordance with the increase of the carriers' concentration due to thermal generation of the split impurity band from the valence band of the glass (Fig. 12).

Another implication of the existence of nanocrystalls in the glass and the DSG is the intensive scattering of the free charge carriers on these pockets of potential energy. This scattering can be as effective as the scattering on dislocations, domain walls and other stretched defects of the crystal lattice [54] because of comparable size of them. Collection of these factors leads to the temperature dependence of the DSG resistivity showed schematically in Fig. 1.

Energy gap E_G between the impurity band and valence band of the glass (Fig. 13*a*) may be considered as pseudogap (Fig. 17), widely used in physics of high-T superconductors [55,56] and originated in our case from fluctuations of impurity distribution and glass disorder. One can assume that the distribution of density of states in the impurity band is Gaussian with the center at $E_i \approx 10^{-2}$ eV and width of $\chi \approx 5$ meV (see above) so tail of pseudogap at the top of valence band $E = E_v$ has density of states $N(E_v) \approx 0.01N(E_i) \approx 10^{18}$ $eV^{-1}cm^{-3}$, i.e. all states in the pseudogap are degenerated. There is another situation at T > 700 K, when structure transitions of nanocrysals have completed: even in the glass 2 doped by 30 wt % of RuO_2 activation energy of conductivity is $E_\sigma \approx 0.047$ eV and $N(E_v) \approx 10^{-30}N(E_i)$ and pseudogap becomes a real gap.

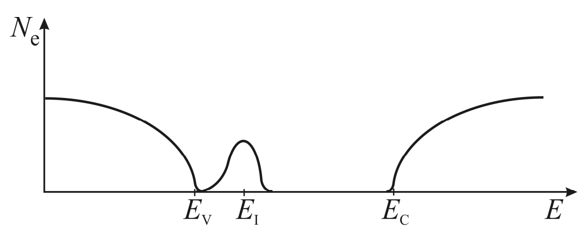

Fig. 17. Pseudogap in the DSG

5. WHY IS THE MINIMUM ON TEMPERATURE DEPENDENCE OF RESISTIVITY OF DSG?

It was shown in previous section that the resistivity of the doped silicate glass is proportional to $\exp(-aT^{\varsigma})$ at low temperatures (T < 50 K), 0.4 < ζ < 0.8 due to coexistence of impurity band and nanocrystals. Structural transitions of nanocrystals take place at high temperatures (T > 800 K) and the conductivity of the doped silicate glass decreases sharply (region III in Fig. 1, and Fig. 15).

We will consider now the origin of the minimum in the temperature dependence of resistivity (region II in Fig. 1). It is shown [54] that the minimum arises from merge of impurity band into the valence band of glass at temperature high enough, so thermal activation of charge carriers as well as its hopping are failed, and scattering of free charge carriers become predominant factor in the temperature dependence of the resistivity.

Leitmotiv of the most commonly discussions of conduction mechanisms of DSG is [9] "TFR may be regarded as belonging to the general class of colloidal composite, where the conducting particles are dispersed into a continuous insulating matrix. Thermal processing in the fabrication of TFR has the primary effect of softening the glassy phase so as to induce wetting of the conducting particles. As a result, there is usually no physical contact between adjacent conducting fillers, which instead are separated from each other by a thin glassy layer… In these cases, the resulting changes in the local chemical and physical properties can be tentatively described by considering the conducting particles as coated by a third, thin, phase that changes the local charge distribution." Inconsistency of such an approach has been showed earlier (subsection 3.1).

Recently Murthy [10] has carried out experiments to find a correlation with existing models of electrical conduction in DSG but do not conclude which model is more adequate.

Combination of insulating (the glass) and metallic (the dopant) conductivity in the form

$$\rho(T) = \rho_{g0}\exp(E_{\sigma}/2kT) + \rho_{d0}(1+\alpha T) \tag{14}$$

is used often to describe "metallic" temperature dependence of conductivity of DSG. Here σ_{g0} and E_{σ} are initial ($T \to \infty$) conductivity and activation energy of the glass, ρ_{d0} and α are resistivity of dopant particle and its temperature coefficient. So we will now consider how much this combination is agreed with experiment.

5.1 Combination of the Metallic and Thermal Activated (Semiconducting) Conductivity

Let us to consider the DSG containing C_m = 16 wt% of RuO_2 and 84 wt% of lead-silicate glass 2. C = 9.9% and the mean distance between centers of spherical particles of the dopant (7) is about 0.87 μm for its diameter D = 0.5 μm here. DSG is the foil of $l{\cdot}w{\cdot}t$ = 10.10.0.025 mm^3. Here w, l, t are width, length and thickness of the sample accordingly. t = 0.0025 cm is the standard thickness of the thick film resistors.

Specific weights are γ_d = 6.85 g/cm^3 for the dopant (RuO_2) and γ_g = 4 g/cm^3 for the glass. Resistivity is $\rho_d = 4{\cdot}10^{-5}$ Ohm·cm (RuO_2) and $\rho_g > 10^{16}$ Ohm·cm (the glass). Volume of the sample is $v = 2.5{\cdot}10^{-3}$ cm^3, volume of the dopant is $v_d = Cv = 0.099{\cdot}2.5{\cdot}10^{-3} \approx 2.5{\cdot}10^{-4}$ cm^3.

We will estimate now the upper and lower limits of the resistivity for the DSG sample. There are two extreme distributions of the dopant particles in the sample (Fig. 18). Resistivity of the sample will be intermediate for all other cases.

In the first case the dopant forms the solid film of length l and thickness t along the electric field, i.e. the film closes the metallic terminations (Fig. 18*a*). Resistance of the sample will be

$$R(T) = (((R_0(1 + \alpha T))^{-1} + (b\exp(E_{\sigma}/kT))^{-1})^{-1} \tag{15}$$

Wideness of the same film is $w_d = Cw$ = 0,099 cm and its resistance is $R_{d1} = \rho_d l/(w_d \cdot t) = 4 \cdot 10^{-5}/(0.099 \cdot 2.5 \cdot 10^{-3})$ = 0,162 Ohm. Resistance of the glass film connected in parallel is $R_{g1} = \rho_g l/((1\text{-}w_d) \cdot t) = 10^{16}/(2.5 \cdot 10^{-3} \cdot 0.901) = 4.4 \cdot 10^{18}$ Ohm. One can see that the full resistance of the sample $R_1 = (R_{d1}^{-1} + R_{g1}^{-1})^{-1}$ = 0,162 Ohm is determined by the resistance of the dopant film only.

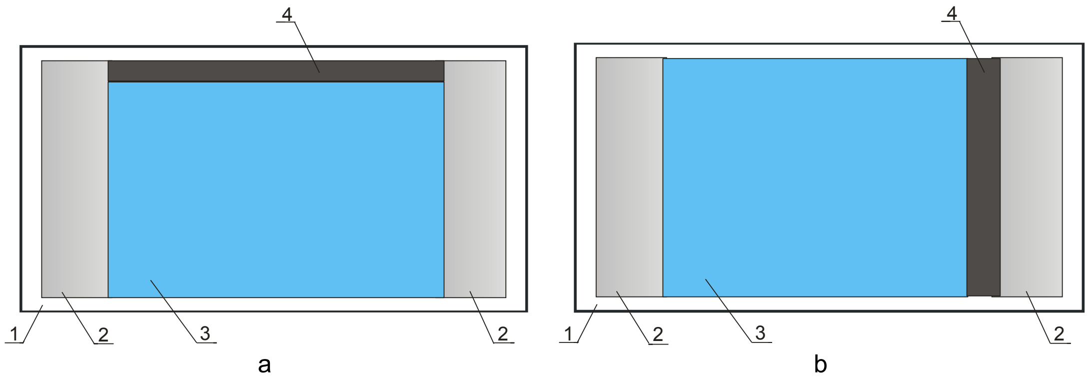

Fig. 18. Configuration of the DSG sample for dopant layer along (*a*) and transverse (*b*) the electric field. 1 is the substrate, 2 is the metallic terminations, 3 is the glass layer and 4 is the RuO_2 layer

In the second case the dopant film is across the electric field (Fig. 18*b*) and its resistance is $R_{d2} = \rho_d w_d/(w \cdot t) = 4 \cdot 10^{-5} \cdot 0.099/2.5 \cdot 10^{-3} = 1.58 \cdot 10^{-3}$ Ohm. The resistance of the glass layer in series is $R_{g2} = \rho_g(1\text{-}w_d)/(w \cdot t) = 10^{16}\, 0.901/2.5 \cdot 10^{-3} = 3.6 \cdot 10^{18}$ Ohm and the total resistance of the sample $R_2 = R_{d2} + R_{g2} = 1.58 \cdot 10^{-3} + 3.6 \cdot 10^{18} = 3.6 \cdot 10^{18}$ Ohm is determined by the glass film resistance. Accordingly, the temperature dependence of the sample resistance is determined by the dopant layer in the first case and by the glass layer in the second case:

$$TCR_1 = dR_1 / (R_0 dT) = d(1+\alpha\Delta T)/dT = \alpha \tag{16}$$

and

$$TCR_2 = dR_2 \big/ (R_{20} dT) = -E_a \exp(E_a \Delta T / 2kT_0 T) \big/ (2kT^2) \tag{17}$$

Here R_0 and R_{20} are values of resistance at some reference temperature T_0, $\Delta T = T - T_0$ is the deviation of temperature from T_0. The minimum of the (13) is possible only if

$$\alpha > \left| -E_a \exp(E_a \Delta T / 2kT_0 T) \big/ (2kT^2) \right| \tag{18}$$

near the minimum.

Simulation of the temperature dependence of the DSG resistance in these cases is shown in Fig. 19*a*. In the case of the dopant layer along the electric field $R(T)$ is linear at low temperatures and has the maximum instead of the experimental minimum so this case is not applicable for DSG.

For this reason we will consider now the metallic and semiconducting sections connected in series (Fig. 18*b*) and attempt to find out the correlation between the resistivity values of these sections at the minimum of the total resistivity. For this purpose we rewrite (9):

$$\rho(T) = a\rho_{g0} \exp(E_a / 2kT) + (1-a)\rho_{d0}(1+\alpha T), \tag{19}$$

here a and $1-a$ are the contributions of the semiconducting and metallic sections to the total resistivity. The condition of the minimum $d\rho(T)/dT = 0$ at $T = T_m$ gives a as a function of T_m:

$$a(T_{\mathrm{m}}) = \left(1 + \frac{1}{\alpha}\frac{\rho_{\mathrm{g0}}}{\rho_{\mathrm{d0}}}\frac{E_{\sigma}}{2kT_{\mathrm{m}}^{2}}\exp\frac{E_{\sigma}}{2kT_{\mathrm{m}}}\right)^{-1}. \tag{20}$$

a (T_m) as function of T_m is showed in Fig. 19*b*. One can see that a ≈ 0.3 – 0.9 is required to have T_m ≈ 300 K, as it has often observed experimentally, and $\rho(T_m)$ must be in order of the $\rho_{g0}(T_{\mathrm{m}})\exp(E_{\mathrm{a}}/2kT_{\mathrm{m}})$ as well as $\rho_{d0}(1+\alpha T_{\mathrm{m}})$. But this condition cannot be realized in the DSG, where ρ_d(300 K) ≈ $4\cdot10^{-5}$ Ohm·cm for RuO_2 and ρ_g(300 K) > 10^{16} Ohm·cm for the glass $2SiO_2\cdot PbO$ while ρ(300 K) ≈ 10^{-2} – 10^{4} Ohm·cm for DSG. It means that the resistivity of RuO_2 or other dopant particles cannot be used for interpret $\rho(T_m)$ in terms of the (14) and the physical or chemical mechanism for reducing of the glass resistivity down to ρ(300 K) should be considered here.

5.2 A Model of Cooperating of Impurity Band and Nanocrystals

5.2.1 The model and simulations

It was pointed out above that the resistivity of the RuO_2 used in DSG is lower of the resistivity of the DSG by factor of 10^3 – 10^4. As a result the mechanism for lowering the ρ_g from 10^{16} Ohm·cm down to the ρ of DSG (at least in order of value) should be considered.

Any of the tunneling of free carriers though the glass interlayer or hopping of them from the one dopant particle to another cannot reduce the glass resistivity down to resistivity of the DSG as well as provide the $R(T)$ with the minimum.

Therefore observed properties of the DSG can be caused by doping of the glass interlayer between the dopant particles due to diffusion of the dopant atoms only [54], and the “metallic” temperature dependence $\rho(T) \sim T$ or $\rho(T) \sim T^2$ should be the property of the doped glass but no that of the RuO_2 particles. This condition is satisfied for the electron-phonon or the electron-electron scattering when electron concentration is constant.

So let us to consider now the combination of thermal activation, hopping and scattering of charge carriers as the main conduction mechanism of the DSG.

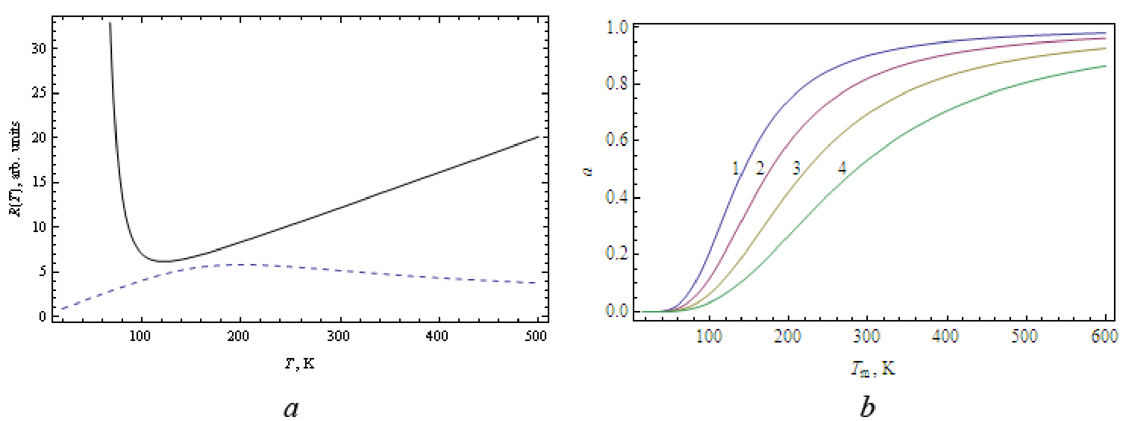

Fig. 19. (*a*) Simulation of the *R*(*T*) of the DSG for the dopant layer, orientated along (15) (dashed line) and across (19) the electric field (solid line) for R_0 = 0.1, α = $4\cdot10^{-3}$, *b* = 1.7, E_σ = 0.45 eV. *b* = 0.02 for (19) with sane other values; (*b*) Contribution of the semiconducting section *a* vs. the temperature of minimum T_m for E_σ = 50 meV, α = 0.004 $K^{-1}$and ρ_{g0}/ρ_{d0}: $6.7\cdot10^8$ (1); $1.35\cdot10^9$ (2); $2.7\cdot10^9$ (3); $5.4\cdot10^9$ (4)

As reported earlier [11] the nanocrystals of silicates in the glass and narrow impurity band formed in firing process can explain the experimental [4,7] low-temperature resistance of DSG in the form (10) without the first term (Mott's law) if the temperature dependence of the energy gap between the impurity band and the valence band of the glass is taken into account.

It is should be noted that the temperature dependence (12) with ς = 0.5 takes place in the hopping model of the doped semiconductors as the result of the Coulomb gap in the energy spectrum of the electrons as well [42] but it was noted ibid, that such a consideration is qualified in the crystalline semiconductors and Coulomb gap is not effective in amorphous materials.

We have taken into account therein the temperature dependence of width $E_G(T)$ of the band-gap between the top of the glass valence band and the impurity band bottom caused by electron-phonon coupling [50,58-62]:

$$E_{\mathrm{G}}(T) \approx E_{\mathrm{G}}(0) - \varsigma T^2 \tag{21}$$

and the temperature coefficient ς is about 10^{-6} eV·K^{-2}, so this effect is not essential in the wide-band semiconductors such as Ge, Si, GaAs or C (diamond). Here $E_G(0)$ is the width of the band gap at T = 0 K.

Expression (21) is the experimental and do not suitable enough at low temperatures ($T < \Theta_D$, here Θ_D is the Debye temperature).

The expression (12) [50] is more correctly at $kT < \langle \hbar\omega \rangle$, and the electron-phonon coupling narrows the band gap E_G (Fig. 13*a*) and last one disappears at the some temperature T_m in the semiconductors having the narrow band gap (less than 10 – 50 meV) [57] (Fig. 13*b*):

$$E_{\mathrm{G}}(T_{\mathrm{m}}) = 0. \tag{22}$$

$$T_{\mathrm{m}} = \frac{\langle \hbar\omega \rangle}{k \ln(1 + 2\xi \langle \hbar\omega \rangle / E_{\mathrm{G}}(0))}. \tag{23}$$

The impurity band and the valence band merge and form unite partially filled valence band as in the metals (Fig. 13*b*) at $T \geq T_m$, so concentration of the charge carriers become constant. The main factor of the temperature dependence of resistivity of the DSG is thereafter the charge carriers scattering on phonons, neutral and ionized impurities or on the other charge carriers, which lead to "metallic" conductivity

$$\rho(T) \sim T\ , \tag{24}$$

$$\rho(T) \sim T^2 \tag{25}$$

or

$$\rho(T) \sim T^{-3/2}. \tag{26}$$

Shifting of the impurity band into the glass band-gap at high temperatures is shown in Fig. 13*c*. Temperature dependence of the impurity band-gap E_G is shown in Fig. 20*a*.

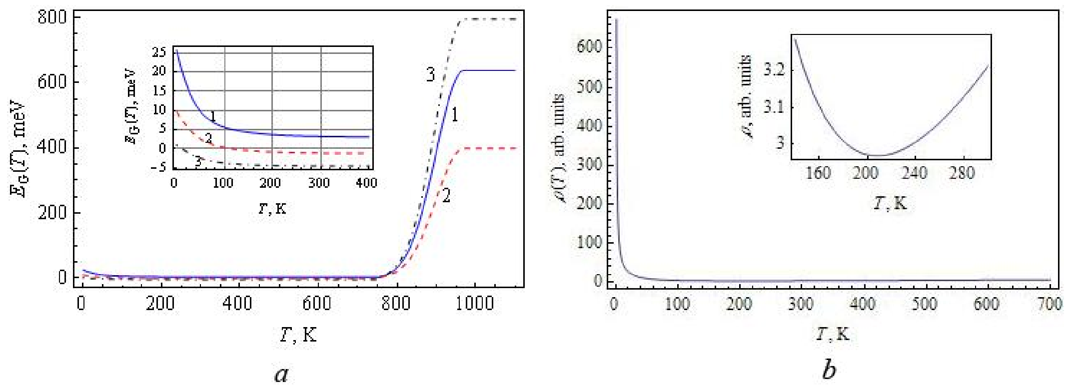

Fig. 20. (*a*) Band-gap width E_G versus temperature including the equation (12) (T < 200 K) and structure transitions of silicate nanocrystals (T > 800 K). Inset is the enlarged part of the main curves. Curves 1, 2 and 3 are responsible for the various width of the band gap at T = 0 K and beyond the 900 K (structure transitions have been completed, see [30]); (*b*) Simulation of the $\rho(T)$ (27) for $A = 10^{40}$; B = 3.5; T_h = 100 K; $E_G(0) = 10^{-2}$ eV; $\langle \hbar\omega \rangle = 22.5$ K; ζ = 0.5. The inset is the enlarged region near the minimum

Thermal activation and hopping of the charge carriers act simultaneously and increase the DSG conductivity while electron-phonon or electron-electron scattering decreases it so one can write for resistivity of DSG

$$\rho(T) = \left[\sigma_a(T) + \sigma_h(T)\right]^{-1} + \rho_{met}(T), \tag{27}$$

Here

$$\sigma_a(T) = AT\exp[-E_G(T)/2kT] \tag{28}$$

is the conductivity due to thermal activation of carriers,

$$\sigma_h = BT^{0.5}\exp[-(T_h/T)^{1/4}] \tag{29}$$

is the hopping conductivity, and

$$\rho_{met}(T) = \rho_{m0}(1 + \alpha T + \beta T^2 + \gamma T^{-3/2}) \tag{30}$$

is the metallic conductivity, caused by scattering of carriers on neutral defects (ρ_{m0}), phonons (αT), charged impurities ($\gamma T^{3/2}$) or other charge carriers (βT^2) [63,64]. The expression (30) assumes that various scattering processes act simultaneously in the DSG.

It should be emphasized that $\rho_{met}(T)$ is the intrinsic property of the doped glass here in contrary to the (2) and (10), where $\rho_{d0}(1+\alpha T)$ is the parameter of the dopant particles. Expression (27) with (11), (28), (29) and (30) is shown in Fig. 20*b*.

5.2.2 Experimental results and comparison

Comparison of the experimental results of the temperature dependence of the resistance $R(T)$ of the DSG samples and our model (27) in the temperature range 160 – 800 K shows the good agreement (Fig. 21).

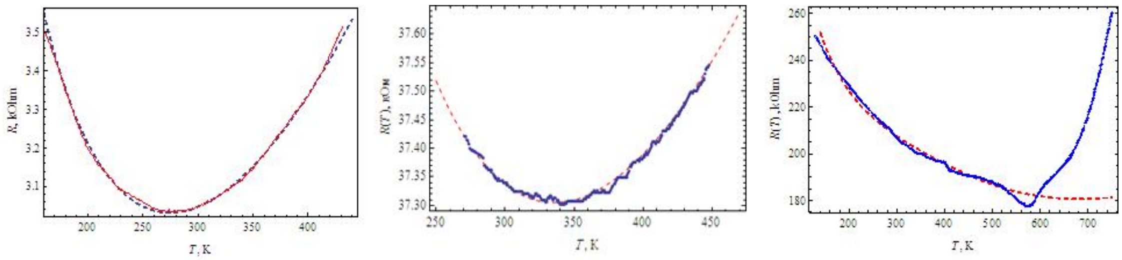

a *b* *c*

Fig. 21. Experimental (blue lines) and simulated (red lines) temperature dependence of resistance of: the DSG1 (*a*), DSG3 (*b*) and DSG2 (*c*). Dopant–RuO_2. The minimum in (*c*) is distorted by the resistivity variations due to structure transitions of the silicate nanocrystals in the glass at $T = 575$ K and $T > 800$ K [30]. Simulation have carried out for the function (27) with (12), (28) – (30) by parameters in table 2

Table 2. Parameters of simulation for Fig. 21

Fig. 21	C_m, wt %	A, $(Ohm{\cdot}K)^{-1}$	$E_G(0)$, eV	ξ	$\langle\hbar\omega\rangle$ meV	B, 10^{-5} $K^{-0.5}$/Ohm	T_h, K	$R_{m0} = \rho_{m0}/t$, kOhm	α, ppm/K	β, 10^6 $Ohm{\cdot}K^{-2}$
a	20	$2.5{\cdot}10^{-7}$	10	1.1	2	1.75	100	1.342	0	3.94
b	16.5	$4.42{\cdot}10^{-7}$	12.3	1.1	4.8	3.91	250	34.85	12	0
c	16	$3.27{\cdot}10^{-8}$	430	0.01	3.86	0.475	1050	158	145	29.52

It is seen from these figures that

i) $R(T)$ of the all investigated DSG is not quadratic (1) in contrast with the opinion in [13-15];
ii) the temperature T_m of the minimum is affected by DSG composition and firing conditions (T_f and τ);
iii) the temperature T_m of the minimum increases with the resistivity ρ of the DSG so can be distorted (Fig. 21*c*) by structure transitions of silicate nanocrystals in the DSG [11].

6. CONCLUSIONS

1. The known conduction mechanisms of the DSG cannot explain the origin of the minimum of the temperature dependence of resistivity and the effect of the glass and dopant composition, firing conditions (T_f and τ) on the its location (temperature T_m and resistivity ρ_m) as well as maximum of resistivity at high temperature.
2. To correctly explain the DSG conduction mechanism, it is necessary to take into account the interaction of glass and dopant during sintering, resulting high conductivity of the glass.
3. Electrical conduction of the DSG is the result of simultaneous acting of impurity band and silicate nanocrystals. Impurity band is generated in sintering due to diffusion of dopant atoms into the glass, while the nanocrystals are native part of the glass.
4. The nanocrystals undergo structural transitions at high temperatures leading to sharply increasing of resistivity of DSG.
5. The minimum of the temperature dependence of the DSG resistivity is the result of electron-phonon interaction, leading to conjugation of impurity band and valence band of the glass. Beyond the minimum “metallic” conductivity may appear due to electrons scattering while their concentration becomes constant.

It is very important here that the impurity band-gap is narrow (about tens of meV) so the band-gap can vanish at temperature T_m near the room temperature (the broad brand-gap will disappear at high T_m and we can't observe its vanishing due to the structural transitions of nanocrystals).

COMPETING INTERESTS

Author has declared that no competing interests exist.

REFERENCES

1. Prudenziati M, Hormadaly J, Editors. Printed Films – Materials science and applications in sensors, electronics and photonics. Cambridge: Woodhead Publishing; 2012.
2. Thick Film Heaters.
   Available:www.watlow.com.
3. Prudenziati M, editor. Thick Film Sensors. Amsterdam: Elsevier Science; 1994.
4. Pike GE, Seager CH. Electrical properties and conduction mechanisms of Ru-based thick-film (cermet) resistors. J. Appl. Phys. 1977;48(12):5152.
5. Smith DPH, Anderson JC. Electron conduction in thick film resistors. Thin Solid Films. 1980; 71:79.
6. Abe O, Taketa Y. Electrical conduction in thick film resistors. J. Appl. Phys. 1991;24:1163.
7. Schoepe W. Conduction mechanism in granular RuO_2-based thick-film resistors. Physica 1990;B165&166:299.
8. Flachbart K, Pavlik V, Tomašovičova N, Adkins CJ, Somora M, Leib J, Eska G. Conduction Mechanism in RuO_2-Based Thick Films. Phys. Stat. Solidi (b). 1998;205:399.
9. Grimaldi C. Conduction Mechanism in printed thick-film resistors. In. Prudenziati M, Hormadaly J, editors. Printed Films – Materials science and applications in sensors, electronics and photonics. Cambridge: Woodhead Publishing; 2012.
10. Murthy KSRC. Evolution of conduction mechanism in thick film resistors. Int. J. Adv. Res. 2019; 7(4):238-256.
    DOI: 10.21474/IJAR01/8811
11. Abdurakhmanov G. On the Conduction Mechanism of Silicate Glass Doped by Oxide Compounds of Ruthenium (Thick Film Resistors). 2. Nanocrystals in the Glass and Charge Carrier's Localization. American J. Materials Science. 2011;1(1):12-17.
    DOI: 10.5923/j. materials.20110101.03
12. Kubovy A. Model of electric conductivity of thick-film resistors. Part III. Temperature Dependence of Sheet Resistivity. Ceramics – Silikaty. I995;39(1):I-40.
13. Prudenziati M, Cattaneo A. Thermoelectric Power in Thick Film Resistors. Electrocomponent Science Technology. 1976;3:181-183.
    DOI:http://dx.doi.org/10.1155/APEC.3.181.
14. Bobran K. et al. Conduction in RuO2-Based Thick Films. International Journal of Electronics. 1995;78:113-119.
    DOI:http://dx.doi.org/10.1080/00207219508926143
15. Forlani F, Prudenziati M. Electrical Conduction by Percolation in Thick-Film Resistors. Electrocomponent Science and Technology. 1976;3:77-83.
    DOI:http://dx.doi.org/10.1155/APEC.3.77.
16. Abdurakhmanov G, Abdurakhmanova NG. High Temperature Anomalies in Resistivity and Thermoelectric Power of Thick Film Resistors. Phys. Stat. Solidi (a). 2005;202(9):1799.
    DOI 10.1002/pssa.200420036
17. Morten B, Prudenziati M, Sacchi M, Sirotti F. Phase transitions in Ru based thick-film (cermet) resistors. J. Appl. Phys. 1988;83:2267.
18. Shelby JE. Introduction to Glass Science and Technology. Cambridge: RSC; 2005.
19. Hodkin FW, Cousen AA. Textbook of Glass Technology. London: Constable and Company Ltd.; 1929.
20. Abdurakhmanov G, Vakhidova G, Tursunov L. Interaction of RuO_2 and lead-silicate glass in thick-film resistors. World J. Condensed Matter Phys. 2011;1(1):1.
21. Vlasov A G, Florinskaya VA et al. Infrakrasnie spektri neorganicheskix stekol I kristallov. – Leningrad: Ximiya Publishing House; 1972. Russian.

22. Lazarev AN. Kolebatelnie spektri I stroenie silikatov. Leningrad: Nauka Publishing House; 1968. Russian.
23. Ginzburg VL. The propagation of electromagnetic waves in plasmas. Oxford: Pergamon Press; 1970.
24. Sidorov TA. Infrakrasnie I ultrafioletovie spektri I structura svintsovosilikatnix stekol. J. Prikladnoy Spektroskopii. 1967;6:98. Russian.
25. Shklovskii BI, Efros AL, Electronic properties of doped semiconductors. Heidelberg: Springer; 1984.
26. Ziman J. Models of Disorder. Cambridge: Cambridge U. Press; 1979.
27. Bonch-Bruevich VL et al. Electron Theory of Disordered Semiconductors. Moscow: Nauka Publishers; 1981. Russian.
28. Grimaldi C, Maeder T, Ryser P, Strässler S. A model of transport nonuniversality in thick-film resistors. arXiv:cond-mat/0307141 v1 7 jul 2003.
29. Abdurakhmanov G. On the Conduction Mechanism of Silicate Glass, Doped by Oxide Compounds of Ruthenium: Diffusion and Percolation Levels. World J. Condensed Matter Physics. 2011;1(1):19.
DOI:http://dx.doi.org/10.4236/wjcmp.2011.12004
30. Lee J, West RW. Firing studies with model thick film resistor systems. IEEE Trans. Comp. Hybrids and Manufact. Technol. 1983;CHMT-6(4):430.
31. Stark JP. Solid State Diffusion. N. Y.: Wiley; 1976.
32. Palanisamy P, Sarma DHR, Vest RW. Solubility of Ruthenium Dioxide in Lead Borosilicate Glasses. J. Amer. Ceramic Soc. 1989;72(9):1755.
33. Schreiber HD, Settle FA jr., Lynne JP, Eckenrode JP, Headley GW. Ruthenium in Glass-Forming Borosilicate Melts. J. Less-Common Metals. 1986;115:145.
34. Pflieger R, Malki M, Guari Y, Larionova J, Grandjean A. Electrical Conductivity of RuO_2–Borosilicate Glasses: Effect of the Synthesis Route. J. American Ceramic Society. 2009; 92(7):1560.
DOI: 10.1111/j.1551-2916.2009.03088.x
35. Jagtap Sh, Rane S, Amalnerkar D. Environmentally sustainable composite resistors with low temperature coefficient of resistance. Microelectronic Engineering Archive. 2009;86(10)2026.
DOI: 10.1016/j.mee.2008.12.092
36. Kolek A et al. Noise and switching phenomena in thick-film resistors. J. Physics D: Applied Physics. 2008;41(2):025303.
DOI: 10.1088/0022-3727/41/2/025303.
37. Totokawa M, Yamashita S, Morikawa K, Mitsuoka Y, Tani T, Makino H. Microanalyses on the RuO_2 Particle–Glass Matrix Interface in Thick-Film Resistors with Piezoresistive Effects. International J. Appl. Ceramic Technology. 2009;6(2)195.
DOI: 10.1111/j.1744-7402.2008.02325.x.
38. Totokawa M, Tani T, Yoshimura M, Yamashita S, Morikawa K, Mitsuoka Y, Nonaka T. Chemical and Piezoresistive Microanalyses at the Interface of RuO_2-Glass Diffusion Pairs. J. American Ceramic Society. 2010;93:481.
DOI:http://dx.doi.org/10.1111/j.1551-2916.2009.03403.x.
39. Hill RM. Electrical transport in thick film resistors. Electrocomp. Sci. Technology 1980;6:141.
DOI:http://dx.doi.org/10.1155/APEC.6.141
40. Eitel W. The Physical Chemistry of the Silicates. Chicago: The University of Chicago Press; 1954.
41. Abdurakhmanov G, Abdurakhmanova N, Tursunov A Vahidova G. Evaluation of the transport parameters of RuO_2 doped lead-silicate glass from optical and infrared spectra. Uzbek Physical J. 2009;11(2)141.
42. Alexandrov D. Heavy electrons in nanostructure clusters of disordered solids. In: ICCF-14 International Conference on Condensed Matter Nuclear Science. Washington, DC; 2008.
Available:http://www.lenr-canr.org/acrobat/Alexandrovheavyelect.pdf.
43. Shakhmin AL, Murashov SB. Electronic structure of the three-component lead-silicate glasses. Technical Physics Letters. 2000;26(3):208-210.
DOI: 10.1134/1.1262793

44. Azniuk YuM, Gomonnay AV, Goyer DB, Megela IG, Lopushansky VV. Effect of high-energy electron irradiation on optical spectra of lead silicate glass. Fizika. 2002;A11(1):51.
45. Leko VK, Mazurin OV. Svoystva kvartsevogo stekla (Properties of the silica glass). Leningrad: Nauka Publishers, Leningrad branch; 1985. Russian.
46. Samsonov GV, editor. Physical and Chemical Properties of the Elements. Handbook. Kiev: Naukova Dumka Publishing House; 1985. Russian.
47. Mott NF, Davis EA. Electron Processes in Non-Crystalline Materials. Oxford: Clarendon Press; 1979.
48. Lewis AJ. Use of Hydrogenation in the Transport Properties of Amorphous Germanium. Physical Review B. 1976;14:658.
DOI:http://dx.doi.org/10.1103/PhysRevB.14.658.
49. Halder NC, Snyder RJ. Measurement of the Tunneling and Hopping Parameters in RuO_2 Thick Films. ElectroComponent Science and Technology. 1984;11:123.
DOI:http://dx.doi.org/10.1155/APEC.11.123.
50. O'Donnell KP, Chen X. Temperature dependence of semiconductor band gaps. Appl. Phys. Lett. 1991;58(25):2924.
DOI: 10.1063/1.104723
51. Libau F. Structural Chemistry of Silicates. Berlin-New York: Springer-Verlag; 1985.
52. Blinc R, Žekš B. Soft modes in ferroelectrics and antiferroelectrics. Amsterdam: North-Holland Pub. Co.; 1974.
53. Semenchenko VK, Baskakova VB. Otermodinamicheskoy stabilnosti kvartsa okolo α- i β-perexodov.Neorganicheskie Materiali. 1969;5(4):766. Russian.
54. Matare HF. Defect Electronics in Semiconductors, New York: Wiley Interscience; 1971.
55. Timusk T, Bryan S. The pseudogap in high-temperature superconductors: an experimental survey. Reports on Progress in Physics. 1999;62(1):61.
arXiv:cond-mat/9905219
56. Ma Yao. Low-temperature pseudogap phenomenon: Precursor of high-Tc superconductivity. New Journal of Physics. 2014;16:083039.
DOI: 1367-2630/14/083039+46$33.00
57. Abdurakhmanov G. On the Conduction Mechanism of Silicate Glass Doped by Oxide Compounds of Ruthenium (Thick Film Resistors). 3. The Minimum of Temperature Dependence of Resistivity. World J. Cond. Matter Phys. 2014;4:166.
DOI:http://dx.doi.org/10.4236/wjcmp.2014.43021
58. Fan HY. Temperature Dependence of the Energy Gap in Monatomic Semiconductors. Physical Review. 1950;78:808.
DOI:http://dx.doi.org/10.1103/PhysRev.78.808.2
59. Fan HY. Temperature Dependence of the Energy Gap in Semiconductors. Physical Review. 1951;82:900.
DOI:http://dx.doi.org/10.1103/PhysRev.82.900.
60. Passler R. Comparison of Different Analytical Descriptions of the Temperature Dependence of the Indirect Energy Gap in Silicon. Solid-State Electronics. 1996;39:1311.
DOI:http://dx.doi.org/10.1016/0038-1101(96)00037-8
61. Muto T, Oyama S. Theory of the Themperature Effect of Electronic Energy Bands in Crystals. Progress of Theoretical Physics. 1950;5:833.
DOI:http://dx.doi.org/10.1143/ptp/5.5.833
62. Bansal KB, Dixit VK, Venkataraman V, Bhat HL. Temperature Dependence of the Energy Gap and Free Carrier Absorption in Bulk InAs0.05Sb0.95 Single Crystals. Applied Physics Letters. 2003;82:4720.
DOI:http://dx.doi.org/10.1063/1.1587002
63. Abrikosov A. Introduction to the Theory of Normal Metals. New York and London: Academic Press; 1972.
64. Kittel C. Introduction to Solid State Physics. 4th Edition. New York: John Wiley and Sons Inc.; 1971.

Biography of author(s)

Gulmurza Abdurakhmanov
National University of Uzbekistan, Uzbekistan.

Research and Academic Experience: MSci in Physics, Saratov State University, Saratov, Russia (1970)
PhD in Physics and Mathematics, Physical-Technical Institute of UzAS, Tashkent, Uzbekistan (1981)
Doctor of Sciences in Physics and Mathematics, Institute of Nuclear Physics of UzAS, Tashkent, Uzbekistan (2014)
In PhD Thesis an unknown phenomenon was discovered in semiconductor diodes affected high frequency electromagnetic wave, namely at microwave (maximum and inversion of the sign of detected voltage as function of applied AC power, hysteresis in the impedance vs power).
Existence of nanocrystals in lead-silicate glass and structure transitions of them at high temperatures as well as dynamics of impurity band formed in the glass due to doping have founded in DSci Thesis. "Metallic conductivity" of thick film resistors has explained.

Research Area: Materials Science (Solid State), Interaction of Electromagnetic Waves and Inhomogeneous Media, Thick Film Resistor Technology, Energy Conversion (Thermoelectricity)

Number of Published papers: 142

Any other remarkable point(s): Project Manager and PI of 13 R & D projects